University of Thi-Qar Journal of Science (UTsci)
ISSN Onlin:2709-0256, ISSN Print: 1991-8690 Volume (8), No.1

Developing The Performance of Double Quantum Dot Solar Cell Structure

Suha Hadi
Dept. of Physics/ College of Science /University of Thi-Qar

Nassiriya/ Iraq

Amin Habbeb Al-Khursan
Nassiriya Nanotechnology Research Laboratory (NNRL)/ Science College/ University of Thi-Qar
Nassiriya/ Iraq
ameen_2all@yahoo.com

***Abstract*— This work proposes a double quantum dot (QD) structure as an intermediate band for developing solar (SC) performance. The density matrix (DEMs) are written for this system, where coupled with the continuity-current equation and solved numerically to obtain the quantum efficiency (QE). Through this modeling, the momentum matrix elements of QD-QD, QD-wetting layer (WL), and WL-barrier transitions are calculated and the orthogonalized plane wave is assumed for WL-QD. This type of formulation is used for the first time and covers more characteristics than the rate equation modeling by addressing the interaction between all the states. Results are simulated both the excitonic and nonexcitonic (electron-hole(eh)) cases and show the importance of adding the QD layer.**

For the eh model, the band-to-band recombination rates are high for least energy difference. The barrier and WL band-to-band recombinations rates are reduced by more than two orders compared to QD rates. The valence band relaxations are of the same order and higher than corresponding conduction band rates. The relaxations between respective states have higher rates than band-to-band rates.

The discrimination between states is increased under the excitonic model due to increasing hole occupation. The recombination rates are reduced with this model while the QD band-to-band recombination rates are increased. In both models, reducing the QD-QD recombinations and increasing all other recombinations increases the QE. The high QD band-to-band rate increases QE. Note that in the excitonic model, smaller rates than in eh model is enough for high QE.

Keywords— double quantum dot solar cell, electron-hole model, excitonic model, recombination rate, band-to-band, quantum efficiency.

I. INTRODUCTION

Quantum dots (QDs) gets an importance for solar cells (SCs) development. QDs are introduced in the SCs through the third generation called intermediate band SCs (IBSCs). (1) QDs are introduced in the host material where the QD band gap becomes an intermediate band gap in that of the host material. (2) maximum energy is preserved through the enhancement of the sunlight harvesting by including sub-band gap photon absorption [1]. The QD states behave as trapping centers, photo generated carriers which are extracted to the bulk states, improving current, and then improving conversion efficiency. This is contradicted by the behavior in the impurity photovoltaics, which limits efficiency [2].

QD solar cells (QDSCs) compromised an InAs QD embedded into the GaAs matrix is studied extensively. Sablon et al. studied nanoscale band engineering of InAs QDs to suppress the capture of photogenerated carriers in QDs [3]. Electron and hole dynamics as excitonic and non-excitonic behavior in InAs/GaAs QDSCs is modeled where the non-additive behavior of the photocurrent for QD and barrier contributions is shown to be eliminated in the case of separate electron-hole behavior [4]. Metal nanoparticles are used for photocurrent increment in the GaAs QDSCs by Foroutan and Baghban [5].

After developing the growing technology and the possibility of growing QDs with different sizes and shapes, double QDs (DQDs) is proposed for improving the QD linear and nonlinear response due the flexibility in manipulating between states [6, 7]. So, a DQD Y-configuration system is proposed in this sense [8]. After that, ladder-plus-Y DQD system by considering wetting layer (WL) with an orthogonalized plane wave (OPW) between QD states and WL is proposed to simulate the real QD structure where OPW cannot be avoided [9]. It is shown that the optical properties and their controlling are improved in this structure [10, 11].

This work proposes DQD solar cells (DQDSCs) to improve solar cell performance. In this work, the energy sub bands of the QDs used in DQD system are calculated. Then, the density matrix equations (DMEs) for the DQDSC are introduced. This type of formulating the system is used for the first time. It is best than the rate equations that are used to modeling solar cells. DMEs give the possibility to formulation the interaction between all the states (and bands) which is not possible with any other modeling type. Through this modeling, the momentum matrix elements of QD-QD, QD-WL, and WL-barrier transitions are calculated. The orthogonalized plane wave is assumed for WL-QD. This is to make the formulation in-line with practice where the overlap between WL-QD wave functions cannot be neglected. Then, the continuity-current equation is used to get an analytical

solution for the current density in the p-, n-, and depletion regions and connecting with the DMEs and solved numerically to obtain the quantum efficiency (QE). This type of formulation is not used in works of other laboratories that formulates solar cell performance. Two types of modeling to examining the DQDSCs are used: The electron-hole (eh) model where the relaxation times from electron and hole states are considered separately which is best for low carrier assumptions. The exciton model is the second one where the electron and hole relaxation times are taken the same, which is good for high carrier concentration. Experimental values of relaxation times are considered.

II. InAs DQD structure

The DQD structure used in the SC structure is composed of two QDs. The shape of each QD is InAs quantum disk of radius a and height h. The size of the first QD is (h= 2 nm, a =14 nm) while that of the second QD is (h=3.5 nm, a =13 nm). Taking the ground state (GS) of each QD in the conduction and valence bands (CB and VB) results in 4 sub bands $|0\rangle,|1\rangle,|2\rangle,\text{and}|3\rangle$. Only a single state for each band in the WL is considered $(|4\rangle\text{and}|5\rangle)$. Additionally, the CB and VB of the barrier are considered. The energy band diagram of the DQDSC structure is shown in Fig. 1.

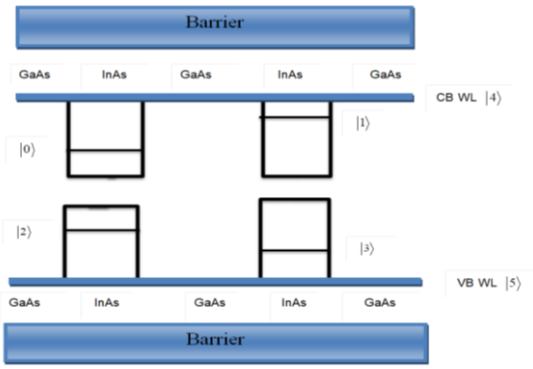

Fig. 1: DQD structure that is used in the solar cell.

III. Derivation of QE in solar cell

The minority carrier-continuity equations for holes in the n-side and electrons in the p-side, respectively, are written as [12, 13],

$$-\frac{1}{q}\frac{\partial J_p}{\partial x}-\frac{\delta p_n}{\tau_p}+G_p=\frac{\partial p_n}{\partial t}, \tag{1}$$

$$\frac{1}{q}\frac{\partial J_n}{\partial x}-\frac{\delta n_p}{\tau_n}+G_n=\frac{\partial n_p}{\partial t}, \tag{2}$$

where the excess hole (electron) concentration due to external excitations is expressed as $\delta p_n = p_n - p_{n0}$, $(\delta n_p = n_p - n_{p0})$, with $p_n(n_p)$ is the total hole (electron) concentration in the n-region (p-region), and $p_{n0}(n_{p0})$ is the hole (electron) concentration without any injection. τ_p and τ_n are the hole and electron lifetimes, respectively. $J_p(J_n)$ is the photocurrent density of holes (electrons) in the n (p) region. The distance-dependent generation rate of the electron-hole pair $G_p(G_n)$ is the photon generation rate in the p-(n-) region at steady state. Introduce the following definitions of the generation rate depending on the[region]:

$$G_{n\ell}=(1-R)\alpha_{n\ell}\Phi\exp\left\{-\left(\alpha_{n\ell}x_j+\alpha_{d\ell}W+\alpha_{p\ell}\left[x-x_j-W\right]\right)\right\}, \tag{3}$$

$$G_{p\ell}=(1-R)\alpha_{p\ell}\Phi\exp\left\{-\left(\alpha_{p\ell}x_j\right)\right\}, \tag{4}$$

where the distance (x) dependent absorption coefficient is α_{p_ℓ}, α_{n_ℓ}, α_{d_ℓ} are the absorption coefficients of the $p-$, $n-$, and depletion layers, respectively, $\ell(=QD,w,B)$ refers to the layers: QD, WL, or barrier, x_j is the junction depth, and W is the depletion width, see Fig. 2, the air-semiconductor optical reflectivity factor is R and Φ is the illuminated photon number. Since the diffusion process is the dominant one for the minority current density, then one can put [13],

$$\frac{-1}{q}\frac{\partial J_p}{\partial x}\square D_p\frac{\partial^2\delta p_n}{\partial x^2} \tag{5}$$

$$\frac{1}{q}\frac{\partial J_n}{\partial x}\square D_n\frac{\partial^2\delta n_p}{\partial x^2} \tag{6}$$

.

Note that Dp and Dn are the diffusion coefficients for the hole and electron. Replacing Eqs. (5) and (6) into Eqs. (1) and (2) which are analytically solved to obtain the relations of the carrier density in the regions. Note that the solution is regarding for QD region only since the main contribution to generation rate comes from the QD layer due to its high absorption compared with WL and barrier. After some manipulations, the relation of the hole density is derived. It is given by [12],

$$\delta p_n=\frac{\alpha_n\phi(1-R)\tau_p}{(\alpha_n^2L_p^2-1)}\{\frac{\cosh(x/L_p)}{\sinh(x_j/L_p)}[e^{-\alpha_n x_j}-\frac{(D_p\alpha_n^2-S_p)}{([D_p/L_p^2]-S_p)}e^{(x_j/L_p)}]+\frac{(D_p\alpha_n^2-S_p)}{([D_p/L_p^2]-S_p)}e^{(x/L_p)}-e^{-\alpha_n x}\} \tag{7}$$

In the above relation; S_p refers to surface recombination velocity of holes. $L_p(=\sqrt{\tau_p D_p})$ is the hole diffusion length. Similarly, the p-region electron density is derived. It is given by [12],

$$\delta n_p=\frac{\alpha_p\phi(1-R)\tau_n}{(\alpha_p^2L_n^2-1)}e^{-(\alpha_n x_j-\alpha_d W)}\{e^{-(x-x_j-W/L_n)}+\frac{\sinh(x-x_j-W/L_n)}{\sinh(H'/L_n)}[(\alpha_p^2-S_n)e^{-\alpha_p H'}]-[\frac{D_n}{L_n^2}-S_n]e^{-H'/L_n}-e^{-\alpha_p(x-x_j-W)}\} \tag{8}$$

where $H' = H - x_j - W$, see Fig. 2. S_n is the surface recombination velocity of electrons. $L_n (= \sqrt{\tau_n D_n})$ is the electron diffusion length. The photocurrent density of holes in the n-region is $J_p \approx -qD_p \frac{\partial}{\partial x}\delta p_n$ and that of electrons in the p-region is $J_n \approx -qD_n \frac{\partial}{\partial x}\delta n_p$. The drift photocurrent density from the depletion region is defined by [13],

$$J_{dr} = q\phi(1-R)e^{-\alpha_n x_j}\left(1-e^{-\alpha_d W}\right) \quad (9)$$

while the QE is defined by the relation [13]

$$QE = \frac{(J_p + J_n + J_{dr})}{q\phi(1-R)} \quad (10)$$

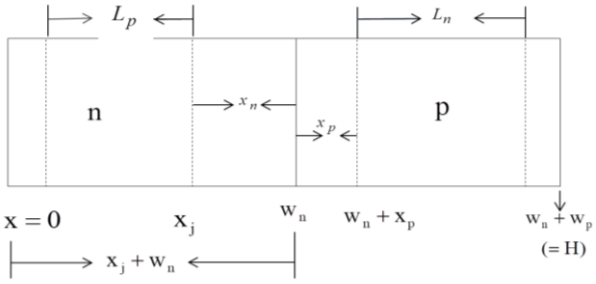

Fig. 2: A schematic representation of the structure of the layers of QD solar cell.

IV. The Dynamical Equations of DQD System

The DQD system Hamiltonian is given by,

$$H = H_0 + H_{\text{int}} + H_{\text{relax}} \quad (11)$$

where H_0 is the unperturbed Hamiltonian, H_{int} is the interaction Hamiltonian while H_{relax} is for relaxations. The unperturbed Hamiltonian is given by

$$H_0 = \sum_{j=0}^{7} \hbar w_j \, |j\rangle\langle j| \quad (12)$$

with $\hbar w_j$ is the jth state energy. The interaction Hamiltonian is given by,

$$H_{\text{int}} = \begin{bmatrix} 0 & -\hbar\beta_{01} & -\hbar\beta_{02} & -\hbar\beta_{03} & -\hbar\beta_{04} & 0 & 0 & 0 \\ -\hbar\beta_{01} & a_{10} & -\hbar\beta_{12} & -\hbar\beta_{13} & -\hbar\beta_{14} & 0 & 0 & 0 \\ -\hbar\beta_{20} & -\hbar\beta_{21} & a_{20} & -\hbar\beta_{23} & 0 & -\hbar\beta_{25} & 0 & 0 \\ -\hbar\beta_{30} & -\hbar\beta_{31} & -\hbar\beta_{32} & a_{30} & -\hbar\beta_{35} & 0 & 0 & 0 \\ -\hbar\beta_{40} & -\hbar\beta_{41} & 0 & 0 & a_{40} & -\hbar\beta_{45} & -\hbar\beta_{46} & 0 \\ 0 & 0 & -\hbar\beta_{52} & -\hbar\beta_{53} & -\hbar\beta_{54} & 0 & a_{56} & -\hbar\beta_{57} \\ 0 & 0 & 0 & 0 & -\hbar\beta_{64} & 0 & 0 & -\hbar\beta_{67} \\ 0 & 0 & 0 & 0 & 0 & -\hbar\beta_{75} & -\hbar\beta_{76} & 0 \end{bmatrix} \quad (13)$$

Note that $\beta_{ij} = \frac{a_{ij}}{2} + \frac{1}{T_2}$ with a_{ij} is the Einstein coefficient $(a_{ij} = \mu_{ij}^2 \omega_{ij}^2 / 3\pi\hbar\varepsilon_0 c^3)$ and T_2 is the dephasing time [14]. Under the density matrix equation,

$$\frac{d\rho}{dt} = -\frac{i}{\hbar}[H, \rho] \quad (14)$$

By using the DQD system Hamiltonian, Eq. 12, under the rotating wave approximation, the dynamical approach for DQD system is written as follow,

$$\dot{\rho}_{00} = -\gamma_{10}\rho_{00} - \gamma_{04}\rho_{00} + \gamma_{40}\rho_{44} + \gamma_{10}\rho_{11} + \beta_{01}(\rho_{10} - \rho_{01}) + \beta_{02}(\rho_{20} - \rho_{02}) + \beta_{03}(\rho_{30} - \rho_{03}) + \beta_{04}(\rho_{40} - \rho_{04}) + G_{n_{QD}} - (U_{02} + U_{03}).$$

$$\dot{\rho}_{11} = -\gamma_{10}\rho_{11} - \gamma_{14}\rho_{11} + \gamma_{11}\rho_{00} + \gamma_{41}\rho_{44} + \beta_{10}(\rho_{01} - \rho_{10}) + \beta_{12}(\rho_{21} - \rho_{12}) + \beta_{13}(\rho_{31} - \rho_{13}) + \beta_{14}(\rho_{41} - \rho_{14}) + G_{n_{QD}} - (U_{12} + U_{13}).$$

$$\dot{\rho}_{22} = -\gamma_{23}\rho_{22} - \gamma_{25}\rho_{22} + \gamma_{32}\rho_{33} + \gamma_{52}\rho_{55} + \gamma_{72}\rho_{77} - \gamma_{27}\rho_{22} + \beta_{20}(\rho_{02} - \rho_{20}) + \beta_{21}(\rho_{12} - \rho_{21}) + \beta_{23}(\rho_{32} - \rho_{23}) + \beta_{25}(\rho_{52} - \rho_{25}) + G_{p_{QD}} - (U_{02} + U_{12}).$$

$$\dot{\rho}_{33} = -\gamma_{32}\rho_{33} - \gamma_{35}\rho_{33} + \gamma_{23}\rho_{22} + \gamma_{53}\rho_{55} + \gamma_{73}\rho_{77} - \gamma_{37}\rho_{33} + \beta_{30}(\rho_{03} - \rho_{30}) + \beta_{31}(\rho_{13} - \rho_{31}) + \beta_{32}(\rho_{23} - \rho_{32}) + \beta_{35}(\rho_{53} - \rho_{35}) + G_{p_{QD}} - (U_{03} + U_{13}).$$

$$\dot{\rho}_{44} = -\gamma_{40}\rho_{44} - \gamma_{41}\rho_{44} - \gamma_{46}\rho_{44} + \gamma_{04}\rho_{00} + \gamma_{14}\rho_{11} + \gamma_{64}\rho_{66} + \beta_{40}(\rho_{04} - \rho_{40}) + \beta_{41}(\rho_{14} - \rho_{41}) + \beta_{45}(\rho_{54} - \rho_{45}) + \beta_{46}(\rho_{64} - \rho_{46}) + G_{n_w} - U_{45}$$

$$\dot{\rho}_{55} = -\gamma_{57}\rho_{55} - \gamma_{52}\rho_{55} - \gamma_{53}\rho_{55} + \gamma_{25}\rho_{22} + \gamma_{35}\rho_{33} + \gamma_{75}\rho_{77} + \beta_{52}(\rho_{25} - \rho_{52}) + \beta_{53}(\rho_{35} - \rho_{53}) + \beta_{54}(\rho_{45} - \rho_{54}) + \beta_{57}(\rho_{75} - \rho_{57}) + G_{p_w} - U_{45}.$$

$$\dot{\rho}_{66} = \frac{A}{q}\left(\frac{dJ_n}{dt}\right) - \gamma_{64}\rho_{66} + \gamma_{46}\rho_{44} + \beta_{64}(\rho_{46} - \rho_{64}) + \beta_{67}(\rho_{76} - \rho_{67}) + AG_{n_B} - U_{67}.$$

$$\dot{\rho}_{77} = -\frac{A}{q}\left(\frac{dJ_p}{dt}\right) - \gamma_{75}\rho_{77} + \gamma_{57}\rho_{55} + \beta_{75}(\rho_{57} - \rho_{75}) + \beta_{76}(\rho_{67} - \rho_{76}) + AG_{p_B} - U_{67}.$$

$$\dot{\rho}_{10} = -\rho_{11}(1-\rho_{00})\tau_{o10}^{-1} - \Delta_{10}\rho_{10} + a_{10}\rho_{00} + \beta_{12}\rho_{20} + \beta_{13}\rho_{30} + \beta_{14}\rho_{40} - \rho_{11}a_{10} + \rho_{12}\beta_{20} + \rho_{13}\beta_{30} + \rho_{14}\beta_{40}.$$

$$\dot{\rho}_{20} = -\rho_{22}(1-\rho_{00})\tau_{o20}^{-1} - \Delta_{20}\rho_{20} + a_{20}\rho_{00} + \beta_{21}\rho_{10} + \beta_{23}\rho_{30} + \beta_{25}\rho_{52} - \beta_{10}\rho_{21} + a_{20}\rho_{22} + \beta_{30}\rho_{23} + \beta_{52}\rho_{25}.$$

$$\dot{\rho}_{30} = -(1-\rho_{00})\tau_{o30}^{-1}\rho_{33} - \Delta_{30}\rho_{30} + a_{30}\rho_{00} + \beta_{31}\rho_{10} + \beta_{32}\rho_{20} + \beta_{10}\rho_{31} - \beta_{20}\rho_{32} + a_{30}\rho_{33}.$$

$$\dot{\rho}_{40} = -(1-\rho_{00})\tau_{o40}^{-1}\rho_{44} - \Delta_{40}\rho_{40} + a_{40}\rho_{00} + \beta_{41}\rho_{10} + \beta_{10}\rho_{41} + a_{40}\rho_{44}.$$

$$\dot{\rho}_{21} = -(1-\rho_{11})\tau_{o21}^{-1}\rho_{22} - \Delta_{21}\rho_{21} + \beta_{20}\rho_{01} + a_{21}\rho_{11} + \beta_{23}\rho_{31} - \beta_{10}\rho_{20} + \beta_{31}\rho_{23} + a_{21}\rho_{22}.$$

$$\dot{\rho}_{23} = -(1-\rho_{33})\tau_{o23}^{-1}\rho_{22} - \Delta_{23}\rho_{23} + a_{23}\rho_{33} + \beta_{25}\rho_{53} + a_{23}\rho_{22} + \beta_{53}\rho_{25}.$$

$$\dot{\rho}_{25} = -(1-\rho_{55})\tau_{o25}^{-1}\rho_{22} - \Delta_{25}\rho_{25} + b_{23}\rho_{35} + a_{25}\rho_{55} - \beta_{35}\rho_{23} - \beta_{25}\rho_{23}.$$

$$\dot{\rho}_{31} = -(1-\rho_{11})\tau_{o31}^{-1}\rho_{33} - \Delta_{31}\rho_{31} + \beta_{30}\rho_{01} + a_{31}\rho_{11} + \beta_{32}\rho_{21} - \beta_{01}\rho_{30} + \beta_{21}\rho_{32} + a_{31}\rho_{33}.$$

$$\dot{\rho}_{35} = -(1-\rho_{55})\tau_{o35}^{-1}\rho_{33} - \Delta_{35}\rho_{35} + \beta_{32}\rho_{25} + a_{35}\rho_{55} - \beta_{25}\rho_{32}.$$

$$\dot{\rho}_{41} = -(1-\rho_{11})\tau_{o41}^{-1}\rho_{44} - \Delta_{41}\rho_{41} + \beta_{40}\rho_{01} + a_{41}\rho_{11} - \beta_{01}\rho_{40} + a_{41}\rho_{44}.$$

$$\dot{\rho}_{46} = -\tau_{o46}^{-1}(1-\rho_{66})\rho_{44} + a_{46}\rho_{66}.$$

$$\rho_{57}^{\square} = -(1-\rho_{77})\tau_{o57}^{-1}\rho_{55} + a_{56}\rho_{77}.$$
$$\rho_{45}^{\square} = -(1-\rho_{55})\tau_{o45}^{-1}\rho_{44} + a_{45}\rho_{55}.$$
$$\rho_{67}^{\square} = -(1-\rho_{77})\tau_{o67}^{-1}\rho_{66} + a_{67}\rho_{77} \quad (15)$$

The diagonal relaxation γ_{jj} is the state $|j\rangle$ relaxation, while γ_{ij} are refer to those between states. $G_{n(p)_\ell}$ refers to the n(p) layer photo-generation rate of QD (WL, barrier) layers, $\ell(=QD, w, B)$, that are defined in Eqs. (3) and (4). $n_{InAs}(n_{GaAs})$ is the intrinsic carrier concentration in the InAs QD (GaAs barrier), they are normalized to the geometrical factors $\frac{h_{QD}}{N_Q}(r_B)$ to attain the intrinsic occupation., that N_Q, h_{QD}, r_B are the QD density, QD height, and density of states (DOS) in the barrier. A is the area of the barrier layer, q is the electronic charge, and $\frac{dJ_p}{dt}(\frac{dJ_n}{dt})$ refers to the time derivative of the hole (electron) current density. $\tau_{r_o}(\tau_{rw})$ is the QD (WL) relaxation rate. Note that this time is also considered for the 3-D barrier layer. The times $\tau_{o_{ij}}$ are the recombination times between states i and j. Δ_{ij} is the frequency difference between states i and j.

V. Recombination Rates

The recombination rates for band-to-band transitions between DQD states are defined as,

$$U_{ij} = (\frac{1}{\tau_{ro}})(\rho_{ii}\rho_{jj} - n_s^2) \quad (17)$$

With $n_s = n_{InAs}\frac{h_{QD}}{N_Q}$ and i refers to the CB QD states $(i = 0, 1)$ and j is refer to the VB QD states $(j = 2, 3)$. For WL and barrier, band-to-band, transitions they are defined by,

$$U_{\ell m} = (\frac{1}{\tau_{rw}})(\rho_{\ell\ell}\rho_{mm} - n_G^2) \quad (18)$$

Note that ℓ refers to the WL (barrier) CB $\ell = 4\,(6)$ and $m = 5(7)$ to the WL (barrier) VB. Then, $n_G = \frac{n_{GaAs}}{r_B}$, $r_B = 2[\frac{2m_o\pi k_\beta T}{\hbar^2}]^{(3/2)}$ is the effective barrier DOS.

The relaxation rate between respective states (or bands) is defined as

$$R_{ij} = \rho_{ii}(1-\rho_{jj})(\frac{1}{\tau_{oij}}) \quad (19)$$

VI. Results and Discussion

A. Relaxation rates

1) eh model at non-Fermi equilibrium

The data used in this work are listed in Tables 1 and 2 for the solar cell structure parameters and in Table 3 for relaxations in the QDSC system. Note that these times are taken from experimental results. Fig. 3 shows the time series of occupation probability of DQD states in addition to the WL and barrier layer. The highest occupations are shown in the barrier layer in the CB and VB $(|6\rangle, |7\rangle)$. As it is taken in the initial conditions, the barrier is assumed to be fully occupied, initially. After this, the occupations are emptied in the CB and decline to half in the VB. The WL is taken as a single state, which is a common assumption in the literature [15, 16]. Fig. 3 shows the raise of WL occupation from zero to ~ half in both CB and VB. Then CB occupation in the WL ρ_{44} goes to near-empty while VB WL occupation ρ_{55} is accomplished into its half value. Our results simulate the expected carrier dynamics between layers (and states). For QD states, the VB DQD states ρ_{22} and ρ_{33} have similar occupations. Although the similar behavior of DQD states is shown, their values are completely different. A high CB occupation for the left QD ρ_{00} compared to that of the right one ρ_{11}. This is acceptable since ρ_{00} is for the CB GS of the DQD system while ρ_{11} is that of ES.

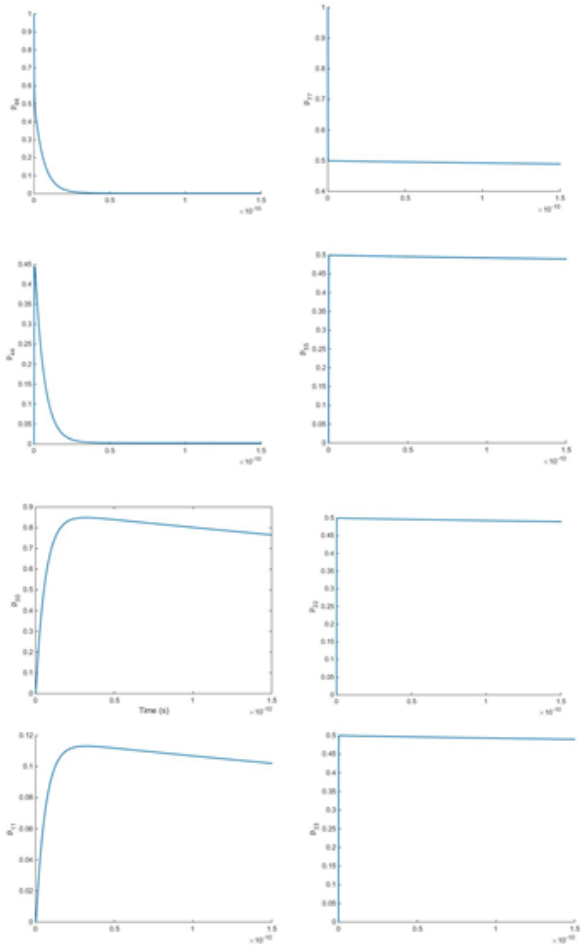

Fig. 3: Time series of DQDSC states.

Fig. 4 shows the carrier occupation of the DQDSC structure versus the junction depth x_j, it continues the scenario plotted in Fig. 3. The barrier and WL occupations are the same in both bands, thus WL occupations are omitted from Fig. 4. The occupation of state $|1\rangle$ is somewhat raising, and then the occupation of $|0\rangle$ state becomes more than half. CB states in QDs, WL, and barrier are decline when the carrier goes deep into the junction. All

VB occupations are ~ similar and raising with junction depth. The VB occupations are fewer raising from barrier to state $|2\rangle$ which is the case of carrier scenario in the DQDSC structure. This figure assess both carrier scenarios and the importance of adding the intermediate band (QD layer). The carriers are relaxes from barrier, to WL, and then to QD states. The highest occupation obtained for long junction depth is 0.645 for ρ_{00} while the lowest one is 2.79×10^{-3} for ρ_{44} in the CB WL.

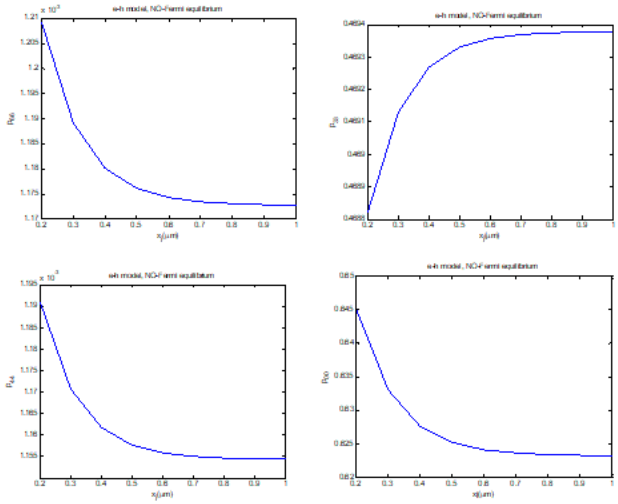

Fig. 4: DQDSC carrier occupation versus the junction depth x_j.

Fig. 5 shows the variation of band-to-band recombination rates versus the junction depth. It is shown that the band-to-band recombination rates are similar between right and left QDs where the recombination rate between QD CB GS, $|0\rangle$, with other two VB QD states $|2\rangle$ and $|3\rangle$, i.e. U_{02}, U_{03} and also U_{12}, U_{13} are the same, so only U_{02} and U_{13} are shown here. It also shows that these recombination are high for the nearest states as in U_{02}. The barrier and WL band-to-band recombination rates U_{67} and U_{45} are reduced by more than two orders compared to QD rates due to long recombination times between these bands compared to QD states. This of course explains the reason for using an intermediate band (QD layer) in solar cells.

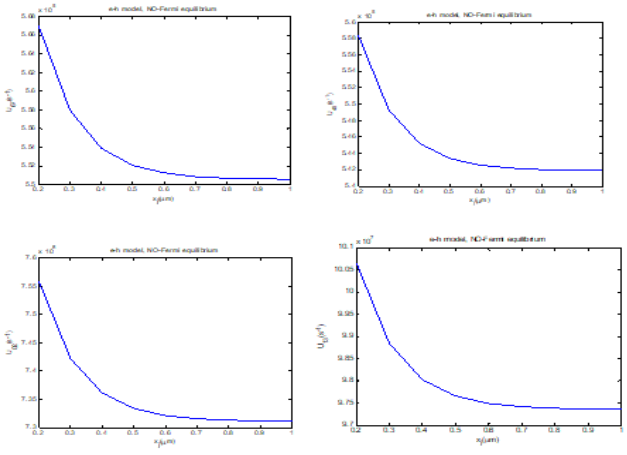

Fig. 5: The band-to-band recombination rates for DQDSC.

Fig. 6 shows the relaxation rates between states. The VB recombination rates R_{57}, R_{35}, R_{23} while those of CB are R_{46}, R_{41}, R_{10}. The VB rates are of the same order (thus R_{35} is not show here) and higher than corresponding CB rates. The rate R_{46} is three orders reduced than VB rates, the rates R_{41} is four orders reduced, while the rate R_{10} is one order reduced. This comes from the higher VB occupations compared to those of CB. Additionally, the relaxation times shown in Table 3 are shorter for holes thus their rates are higher. All recombination rates are increased with their occupations except R_{10} which is reduced with increasing their occupation. This is due to the reduction of ρ_{00} (as shown in Fig. 4) which is the highest occupation in this DQDSC system studied here. One must also refer to the relaxation times $\tau_{10} < \tau_{01}$ compared to all other recombinations, so the rate R_{10} is decline with the occupations of $|1\rangle$ and $|0\rangle$ states. A comparison with the band-to-band recombination rates shows that the relaxations have higher rates.

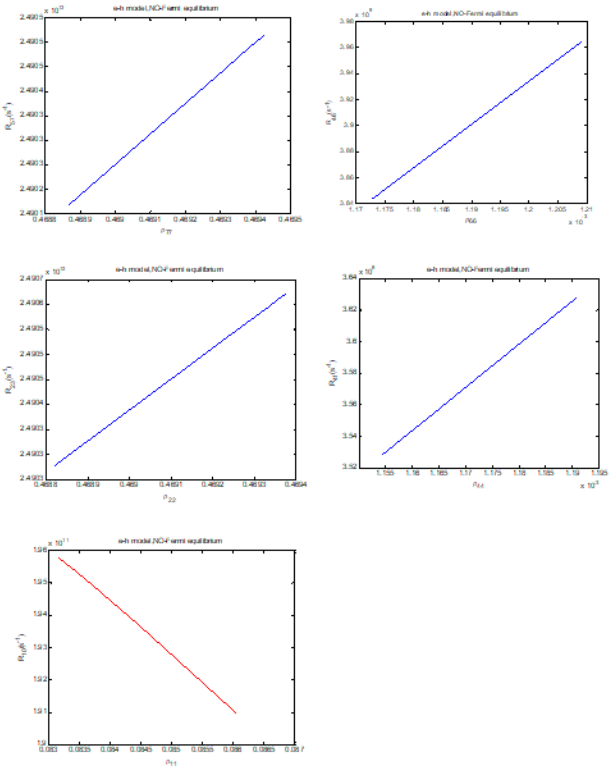

Fig. 6: The relaxation between respective states.

2) Excitonic model at non-Fermi equilibrium

Fig. 7 shows the occupations in the excitonic model, compared with eh model shown in Fig. 4, here ρ_{00} is increased while ρ_{22} is few reduced. The discrimination between states becomes more obvious under the excitonic model which coincides with the results in [4]. Of course this is due to increasing hole occupation as a result of taking its relaxations equal to that of electrons.

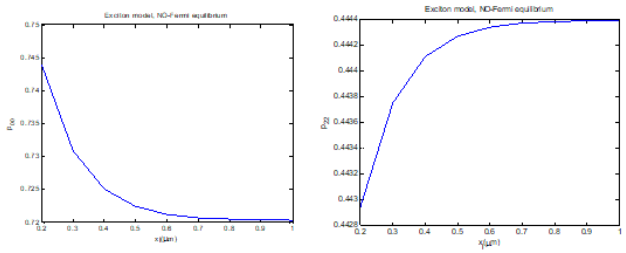

Fig. 7: Occupations versus the junction depth in the excitonic model.

Fig. 8 shows the recombination rates for the excitonic model. The rates are reduced with this model. This of course due to replacing fast hole rates by an excitonic one. In comparison to eh model, while the rate is reduced by one order or more, the reduction is few (~0.2) for the R_{10} recombination.

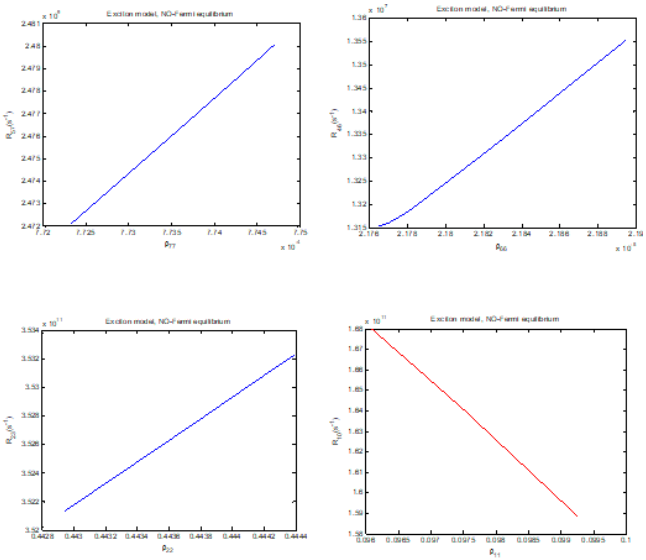

Fig. 8: The recombination rates for excitonic model.

Fig. 9 shows the band-to-band recombination rates in the excitonic model. Compared to eh model, while both barrier and WL rates are reduced the QD rate U_{02} is increased.

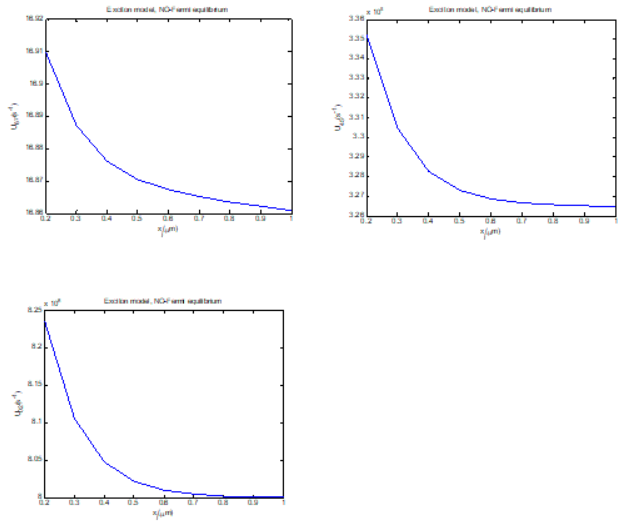

Fig. 9: The band-band recombination rates for excitonic model.

B. *Quantum efficiency*

1) *e-h model*

Fig. 10 shows the quantum efficiency (QE) versus the recombination rates in the eh model. The QE is increased with the R_{46}, R_{41} rates while it is reduced with R_{10} rate. The similarity between all VB recombination rates is obvious, thus only R_{23} is shown. This similarity comes from the similar time used for their transitions. Fig. 11 shows QE versus band-to-band recombination rate in the eh model.

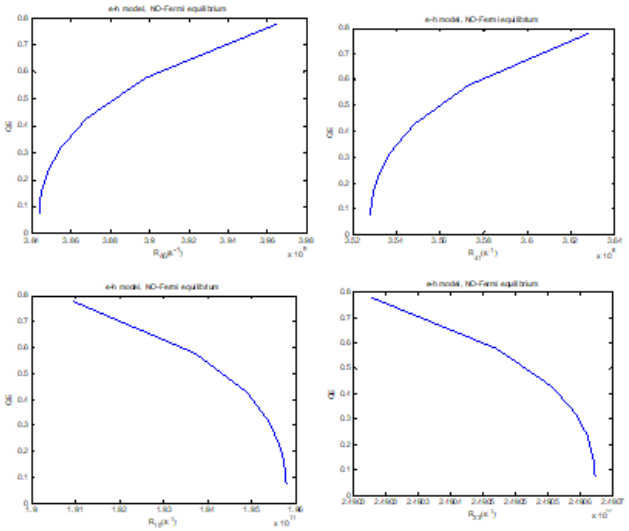

Fig. 10: QE versus recombination rates in the eh model.

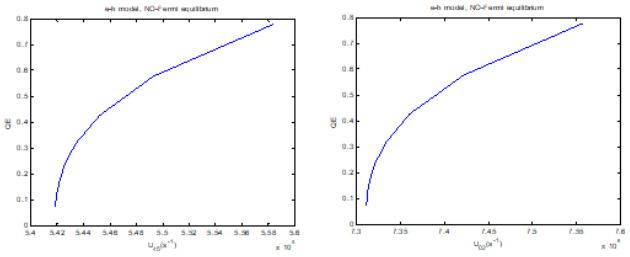

Fig. 11: QE versus band-to-band recombination rates.

2) *excitonic model*

Fig. 12 shows QE in excitonic the model where QE is appearing at rates smaller than that in eh model. It shows that higher QE is obtained with smaller R_{10} rate. Fig. 13 shows QE versus band-to-band recombination rate in the excitonic model. The excitonic model gives a reduction in U_{45} rate and an increment in the U_{02} rate. A note must be put here that the band-band recombination rates are smaller than the recombination rates.

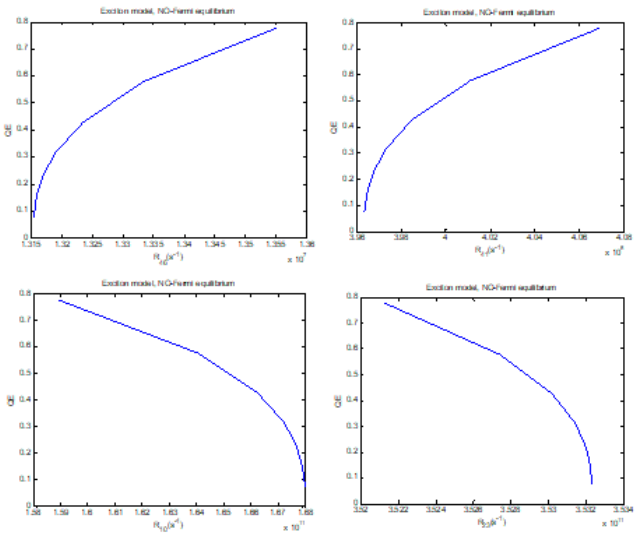

Fig. 12: QE versus recombination rates in the excitonic model.

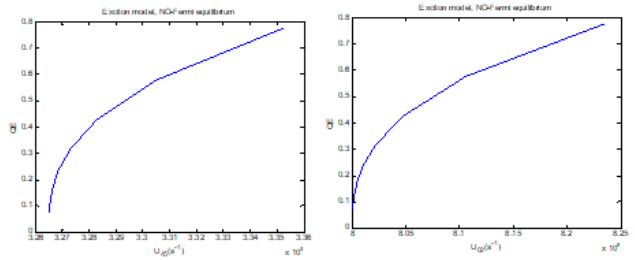

Fig. 13: QE versus band-to-band recombination rates in the excitonic model.

VII. Conclusions

DQDSC structure is proposed for developing solar cell QE. The density matrix equations coupled with the continuity-current equation and solved numerically to obtain QE. Through this modeling, the momentum matrix elements of QD-QD, QD-WL, and WL-barrier transitions are calculated and the orthogonalized plane wave is considered for WL-QD transitions. Results are simulated both the excitonic and eh cases. Through all the results, the importance of adding the QD intermediate band is shown. For the eh model, the carriers are relaxed to QD states. The band-to-band recombination rates are similar between right and left QDs and are high for least energy difference. The barrier and WL band-to-band recombination rates are reduced by more than two orders compared to QD rates due to their long recombination times. The VB relaxation rates are higher than CB rates which increased with their occupations. A comparison with the band-to-band recombination rates shows that the relaxations have higher rates.

The discrimination between states becomes more obvious under the excitonic model due to increasing hole occupation. The recombination rates reduced with this model. the QD band-to-band recombination rates in the excitonic model are increased. In both models, reducing the QD-QD recombination rates and increasing all other recombinations increases the (QE). High QD-QD band-to-band recombination rate increases QE. Note that in the excitonic model smaller rates than that in eh model is enough for high QE.

References

[1] F. Cappellutin, M. Gioannini, A. Khalili, “Impact of doping on InAs/GaAs quantum-dot solar cells: A numerical study on photovoltaic and photoluminescence behavior”, Solar Energy Materials & Solar Cells 157, 209–220 (2016).

[2] M. Gioannini and Ariel P. Cedola, "Simulation of Quantum Dot Solar Cells Including Carrier Intersubband Dynamics and Transport", IEEE J. Photovoltaics 3, 1271-1278 (2013).

[3] K. Sablon, J. Little, N. Vagidov, Y. Li, V. Mitin, and A. Sergeev, “Conversion of above- and below-bandgap photons via InAs quantum dot media embedded into GaAs solar cell”, Applied Physics Letters 104, 253904 (2014).

[4] “A. Cedola, F. Cappelluti and M. Gioannini, “Dependence of quantum dot photocurrent on the carrier escape nature in InAs/GaAs quantum dot solar cells”, Semicond. Sci. Technol. 31, 025018 (2016).

[5] S. Foroutan and H. Baghban, “Theory of plasmonic quantum-dot-based intermediate band solar cells”, Applied Optics 55, 3405-3412 (2016).

[6] J. M. Villas-Bôas, A. O.Govorov, and S. E. Ulloa, “Coherent control of tunneling in a quantum dot molecule”, Phys. Rev. B 69 (2004) 125342.

[7] H. S. Borges, L. Sanz, J. M. Villas-Boas, O. D. Neto, and A. M. Alcalde, “Tunneling induced transparency and slow light in quantum dot molecules,” Phys. Rev. B 85 (2012) 115425.

[8] B. Al-Nashy, S. M. M. Amin and Amin H. Al-Khursan, "Kerr effect in Y- configuration double quantum dot System", J. Opt. Soc. Am. B 31 (2014) 1991-1996.

[9] M. Abdullah, Farah T. Mohammed Noori, and Amin H. Al-Khurasan, "Terahertz emission in ladder plus Y-configurations in double quantum dot structure", Applied Optics 16 (2015) 5186-5192.

[10] B. Al-Nashy, M. Abdullah, Ali Gehad Al-Shatravi, and Amin Habbeb Al-Khursan, "Lasing without population inversion in the four-level Y-type configuration in double quantum dot system", Pramana J. Phys. 91 (2018) 74.

[11] E. Rehman and Amin H. Al-Khursan, "All-Optical Processes in Double Quantum Dot Structure", Applied Optics 55 (2016) 7337-7344.

[12] S. N. Dwara and Amin H. Al-Khursan, "Quantum Efficiency of InSbBi Quantum Dot photodetector", Applied Optics 54, 9722-9727 (2015).

[13] S. N. Dwara and A. H. Al-Khursan, "Two-window InSbBi quantum-dot photodetector", Applied Optics 55, 5591-5595 (2016).

[14] D. Sridharan and E. Waks, “All-Optical Switch Using Quantum-Dot Saturable Absorbers in a DBR Microcavity”, IEEE J. Quantum Electron. 47 (2011) 31-39.

[15] Y. Ben Ezra, B. I. Lembrikov, and M. Haridim, “Specific features of XGM in QD-SOA,” IEEE J. Quantum Electron. 43, 730–737 (2007).

[16] A. H. Flayyih and A. H. Al-Khursan, “Integral gain in quantum dot semiconductor optical amplifiers”, Superlattices Microstruct. 62, 81–87 (2013).